AIAA JOURNAL
Vol. 37, No. 4, April 1999

Plastic Analysis of Complex Microstructure Composites Using the Generalized Method of Cells

Carlos E. Orozco* and Marek-Jerzy Pindera†
University of Virginia, Charlottesville, Virginia 22903

A recently developed computationally efficient implementation of the Generalized Method of Cells is extended here to deal with plasticity problems. The new formulation can be used to perform linear elastic and plastic micromechanical analysis of composites with complex microstructures. It makes use of a tangent plasticity matrix approach as opposed to an initial stiffness matrix approach employed in the original Generalized Method of Cells. This tangent stiffness matrix approach makes it possible to perform plastic analyses of composites with microstructures that require a high-resolution, cell–subcell model. To demonstrate the capabilities of the new formulation, it is applied to the problem of determining the influence of fiber shape and fiber architecture on the plastic behavior of two-phase unidirectional composites. Some results from previous studies on this subject are confirmed. New results that could not be obtained with previous implementations are also reported. Problems modeled with up to 10,000 subcells are presented.

I. Introduction

THE Generalized Method of Cells (GMC)[1,2] is a micromechanics model that has proven to be very effective in modeling the elastic and inelastic behavior of fiber-reinforced unidirectional composites.[3] The method starts by dividing a given cross section of the composite into unit cells that correspond to representative volume elements (RVE). The unit cells or RVE are in turn divided into subdomains called subcells. Figure 1 shows schematically the GMC idealization as applied to a composite lamina. Figure 2 shows a unit cell with the corresponding subcells and the associated nomenclature. The reinforcing fibers are assumed to extend in the x_1 direction. Starting with the material properties of the constituents and the corresponding material constitutive models, the GMC uses traction continuity and compatibility conditions, together with a stress-averaging procedure, to obtain the effective average properties and the effective average behavior of the composite. The GMC is therefore a volume-averaging method that relies on a two-dimensional discretization of the composite in question. Despite the fact that the unit cell is a two-dimensional model, the GMC provides a three-dimensional characterization of the composite in the sense that all of its engineering properties are obtained.

The original GMC formulation is based on an initial stiffness matrix approach. This approach allows for the calculation of the effective linear and/or nonlinear response of a variety of composites with relatively complex microstructures. However, for nonlinear problems the initial stiffness matrix approach is computationally limited to unit cells with about 100 subcells (see Fig. 2).

Motivated by problems that require a much higher resolution (e.g., the problem of tailoring the microstructure of a composite to achieve a certain target response), a high-resolution version of the GMC that allows modeling of the elastic behavior of composites with much more complex microstructures was presented in Ref. 4. This version of the GMC permits the linear elastic analysis of composites with microstructures of up to 10,000 subcells. In this paper this GMC formulation is extended to deal with plastic behavior. As will be apparent from the discussion that follows, the plasticity problem is computationally more challenging than the elastic one. To try to overcome this challenge, a tangent plasticity matrix approach, as opposed to an initial plastic stiffness matrix approach, was used. In addition, the resulting linear systems are stored and solved sparsely, as was done in Ref. 4. The new tangent-sparse formulation not only allows for micromechanical analyses of composites with a variety of accurately modeled fiber shapes and architectures but also provides an opportunity to test the predictive capability of the GMC when the complexity of the microstructures analyzed is pushed to new limits.

Received April 7, 1998; revision received Nov. 10, 1998; accepted for publication Nov. 23, 1998.

*Assistant Professor, Department of Civil Engineering. Member AIAA.
†Professor, Department of Civil Engineering.

II. Effective Elastic Properties

Models of unidirectional composites using the GMC satisfy traction continuity and compatibility conditions in an average sense.[1] Compatibility conditions can be written compactly in matrix form as

$$\boldsymbol{A}_G \boldsymbol{\varepsilon}_s = \boldsymbol{J}\bar{\boldsymbol{\varepsilon}} \tag{1}$$

where $\boldsymbol{\varepsilon}_s \equiv \{\varepsilon^{(11)}, \varepsilon^{(12)}, \ldots, \varepsilon^{(N_\beta N_\gamma)}\}^T$ contains the subcell engineering strains $\varepsilon^{(\beta\gamma)}$ and $\bar{\boldsymbol{\varepsilon}} \equiv \{\bar{\varepsilon}_{11}, \bar{\varepsilon}_{22}, \bar{\varepsilon}_{33}, 2\bar{\varepsilon}_{23}, 2\bar{\varepsilon}_{13}, 2\bar{\varepsilon}_{12}\}^T$ contains the effective average strains in the composite. The matrices $\boldsymbol{A}_G$ and $\boldsymbol{J}$ contain information about the subcells and cell geometry, respectively.

On the other hand, the traction continuity conditions can be written as

$$\boldsymbol{A}_M \boldsymbol{\varepsilon}_s = \boldsymbol{0} \tag{2}$$

where $\boldsymbol{A}_M$ contains entries of the individual elastic stiffness matrices of the subcells. Equations (1) and (2) can be combined into a single equation as follows:

$$\boldsymbol{A}\boldsymbol{\varepsilon}_s = \boldsymbol{K}\bar{\boldsymbol{\varepsilon}} \tag{3}$$

where

$$\boldsymbol{A} \equiv \begin{bmatrix} \boldsymbol{A}_M \\ \boldsymbol{A}_G \end{bmatrix} \tag{4}$$

is a $6N_\beta N_\gamma \times 6N_\beta N_\gamma$ matrix (see Fig. 1) and

$$\boldsymbol{K} \equiv \begin{bmatrix} \boldsymbol{J} \\ \boldsymbol{0} \end{bmatrix} \tag{5}$$

$\boldsymbol{K}$ in Eq. (5) is a $6N_\beta N_\gamma \times 6$ matrix.

For given effective strains, Eq. (3) constitutes a system of $6N_\beta N_\gamma$ equations with $6N_\beta N_\gamma$ unknowns, the solution of which is at the core of the computations in the GMC.

The so-called strain concentration matrix $\boldsymbol{A}_s$ is found as

$$\boldsymbol{A}_s = \boldsymbol{A}^{-1}\boldsymbol{K} \tag{6}$$

where $\boldsymbol{A}$ and $\boldsymbol{K}$ are given by Eqs. (4) and (5), respectively.

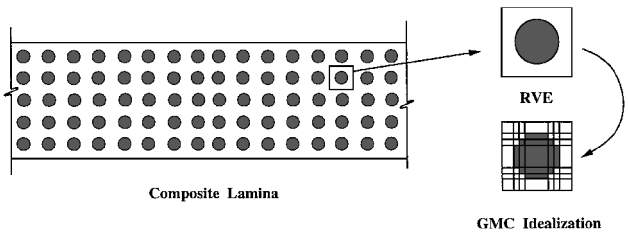

Fig. 1 GMC concept as applied to a composite lamina.

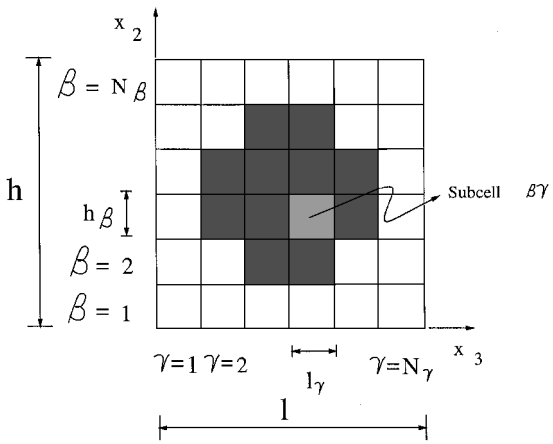

Fig. 2 Repeating unit cell with subcells and nomenclature.

Once $\boldsymbol{A}_s$ is found, the average effective stresses can be calculated as

$$\bar{\boldsymbol{\sigma}} \equiv \frac{1}{hl}\sum_{\beta}^{N_\beta}\sum_{\gamma}^{N_\gamma} h_\beta l_\gamma \boldsymbol{C}^{(\beta\gamma)}\boldsymbol{A}_s^{(\beta\gamma)}\,\bar{\boldsymbol{\varepsilon}} \tag{7}$$

and the effective average stiffness matrix then becomes

$$\bar{\boldsymbol{C}} \equiv \frac{1}{hl}\sum_{\beta}^{N_\beta}\sum_{\gamma}^{N_\gamma} h_\beta l_\gamma \boldsymbol{C}^{(\beta\gamma)}\boldsymbol{A}_s^{(\beta\gamma)} \tag{8}$$

where $\boldsymbol{C}^{(\beta\gamma)}$ is the stiffness matrix corresponding to the material in subcell $(\beta\gamma)$ and $\boldsymbol{A}_s^{(\beta\gamma)}$ is the submatrix of $\boldsymbol{A}_s$ that corresponds to subcell $(\beta\gamma)$.

III. Effective Plastic Response Using the Initial Stiffness Approach

To allow for plastic behavior, in addition to finding $\boldsymbol{A}_s$ in Eq. (6), it is necessary to find $\boldsymbol{A}^P$ as

$$\boldsymbol{A}^P = \boldsymbol{A}^{-1}\boldsymbol{A}^M \tag{9}$$

where

$$\boldsymbol{A}^M \equiv \begin{bmatrix} \boldsymbol{A}_M \\ \boldsymbol{0} \end{bmatrix} \tag{10}$$

Once $\boldsymbol{A}^P$ is obtained, the effective plastic strain in the composite is calculated as

$$\bar{\boldsymbol{\varepsilon}}^P = -\frac{1}{hl}\bar{\boldsymbol{C}}^{-1}\sum_{\beta}^{N_\beta}\sum_{\gamma}^{N_\gamma} h_\beta l_\gamma \boldsymbol{C}^{(\beta\gamma)}\left[\boldsymbol{A}^{P(\beta\gamma)}\boldsymbol{\varepsilon}_s^P - \boldsymbol{\varepsilon}^{P(\beta\gamma)}\right] \tag{11}$$

where $\boldsymbol{A}^{P(\beta\gamma)}$ is the submatrix of $\boldsymbol{A}^P$ that corresponds to subcell $(\beta\gamma)$ and the vector $\boldsymbol{\varepsilon}^P$ contains the plastic strains in all subcells.

Finally, the effective response of the composite can be found as

$$\bar{\boldsymbol{\sigma}} = \bar{\boldsymbol{C}}(\bar{\boldsymbol{\varepsilon}} - \bar{\boldsymbol{\varepsilon}}^P) \tag{12}$$

The main difficulty with the initial matrix approach is that $\boldsymbol{A}^P$ is a $6N_\beta N_\gamma \times 6N_\beta N_\gamma$ fully populated matrix. To store it completely for a problem with 2500 subcells would require 1.8 Gbytes of memory (using double precision). The matrix $\boldsymbol{A}$ in Eq. (6) is of the same size as $\boldsymbol{A}^P$. However, $\boldsymbol{A}$ is sparse, and only the nonzero entries need to be stored. This fact has been exploited in Ref. 4 and has been used to find the effective elastic properties of composite microstructures modeled with up to 10,000 subcells.

To solve the plasticity problem, it is necessary to store $\boldsymbol{A}$ sparsely and, in addition, to avoid having to store $\boldsymbol{A}^P$. This is accomplished by using the tangent plasticity version of the GMC, which is briefly described next.

IV. Effective Plastic Response Using the Tangent Plasticity Matrix Approach

When the tangent plasticity matrix $\bar{\boldsymbol{C}}^P$ is available, an equation equivalent to Eq. (12) is

$$d\bar{\boldsymbol{\sigma}} = \bar{\boldsymbol{C}}^P d\bar{\boldsymbol{\varepsilon}} \tag{13}$$

in which $d\bar{\boldsymbol{\varepsilon}}$ is the total strain increment in a given load step. The procedure to find the plastic response is then an iterative one in which the stress increments are found for a given load history of strain increments $d\bar{\boldsymbol{\varepsilon}}$. The effective stress response is updated at each load step as

$$\bar{\boldsymbol{\sigma}}_{i+1} = \bar{\boldsymbol{\sigma}}_i + d\bar{\boldsymbol{\sigma}} \tag{14}$$

$\bar{\boldsymbol{C}}^P$ in Eq. (13) is the effective tangent plasticity matrix of the composite found using

$$\bar{\boldsymbol{C}}^P \equiv \frac{1}{hl}\sum_{\beta}^{N_\beta}\sum_{\gamma}^{N_\gamma} h_\beta l_\gamma \boldsymbol{C}^{P(\beta\gamma)}\boldsymbol{A}_s^{(\beta\gamma)} \tag{15}$$

where $\bar{\boldsymbol{C}}^{P(\beta\gamma)}$ is the effective tangent plasticity matrix of the material in subcell $(\beta\gamma)$. Notice that Eq. (15) is the same as Eq. (8) except that tangent stiffness matrices are used instead of initial stiffness matrices. Also, the matrices $\boldsymbol{A}_s^{(\beta\gamma)}$ in Eq. (15) are obtained from Eq. (6), but in this case $\boldsymbol{A}$ is assembled using the current tangent stiffness matrices $\boldsymbol{C}^{P(\beta\gamma)}$. An expression for the tangent stiffness matrix is[5]

$$\boldsymbol{C}^{P(\beta\gamma)} = \boldsymbol{C}_0^{(\beta\gamma)} - \frac{\left[\boldsymbol{C}_0^{(\beta\gamma)}\dot{\boldsymbol{\varepsilon}}^P\right]\boldsymbol{s}^T}{\dot{\boldsymbol{\varepsilon}}^T\boldsymbol{s}} \tag{16}$$

where $\boldsymbol{s}$ is a vector of subcell deviatoric stresses, $\dot{\boldsymbol{\varepsilon}}$ is a vector containing the plastic strain rates, and the superscript T stands for transpose. The subcell deviatoric stress vector can be defined as

$$\boldsymbol{s} \equiv \{\sigma_{11} + p, \sigma_{22} + p, \sigma_{33} + p, \sigma_{23}, \sigma_{12}, \sigma_{13}\}^T \tag{17}$$

where $p \equiv -\frac{1}{3}(\sigma_{11} + \sigma_{22} + \sigma_{33})$ is the pressure and the σ_{ij} are the subcell stresses.

The complete procedure to find the plastic strain increments and the plastic strain rate is presented in Sec. V.

Because at each increment of the iterative procedure the individual $\boldsymbol{C}^{P(\beta\gamma)}$ change, it is necessary to solve a system like Eq. (6) at each incremental step to find the current concentration matrix $\boldsymbol{A}_s$. The solution of a single plasticity problem can take hundreds of factorizations of $\boldsymbol{A}$. It is necessary then to take advantage of the sparsity of this matrix. Details about the structure of $\boldsymbol{A}$ and about the way it is assembled can be found in Ref. 4. Once the relevant matrices in Eq. (6) are properly assembled and stored, the solution of the linear systems is obtained with the aid of the ma28.f package from the Harwell Subroutine Library.[‡]

The new effective plastic strain in the composite can be found at the end of each time step as

$$\bar{\boldsymbol{\varepsilon}}_i^P = \bar{\boldsymbol{\varepsilon}}_{i-1} - \bar{\boldsymbol{C}}_0^{-1}\bar{\boldsymbol{\sigma}}_{i-1} \tag{18}$$

Equation (18) is important because it provides a means to calculate the effective plastic strain without having to resort to Eq. (11), which as mentioned before is both storage and computationally inefficient.

[‡]Available from netlib at http://www.netlib.org/index.html.

V. Plastic Strain Incremental Procedure

The procedure to obtain the plastic strain increments is based on that of Mendelson.[6] It constitutes a main component of the general solution algorithm presented in Sec. VI. As described here, it is applicable to homogeneous, isotropic materials.

First, the so-called modified strains are defined as

$$\varepsilon'_i = \varepsilon_i - \varepsilon^P_{i-1} \tag{19}$$

where the subindex i corresponds to the loading step. Then a vector of deviators of the modified strains is calculated as

$$\boldsymbol{e} \equiv \{\varepsilon'_{11} - d, \varepsilon'_{22} - d, \varepsilon'_{33} - d, \varepsilon'_{23}, \varepsilon'_{12}, \varepsilon'_{13}\}^T \tag{20}$$

where $d \equiv \frac{1}{3}(\varepsilon_{11} + \varepsilon_{22} + \varepsilon_{33})$ is the dilatation and the ε_{ij} and ε'_{ij} are subcell total and modified strains, respectively.

The equivalent modified total strain is defined in terms of the modified strain deviator components as

$$\varepsilon_{et} = \left(\tfrac{2}{3}\right)^{\frac{1}{2}}\left[(e_{11})^2 + (e_{22})^2 + (e_{33})^2 + 2(e_{23})^2 + 2(e_{13})^2 + 2(e_{12})^2\right]^{\frac{2}{3}} \tag{21}$$

The change in the equivalent plastic strain is now found as

$$\Delta\varepsilon^P_e = \frac{3G\varepsilon_{et} - \sigma_{e,i-1}}{3G + H_{i-1}} \tag{22}$$

where G is the shear modulus of the material, σ_e is an effective stress (not to be confused with the effective average stress of the composite), and H is the strain hardening slope. The subindex $i-1$ refers to the previous loading step. The current equivalent plastic strain is found as

$$\varepsilon^P_{e,i} = \varepsilon^P_{e,i-1} + \Delta\varepsilon^P_e \tag{23}$$

and the new $\sigma_{e,i}$ can be computed as

$$\sigma_{e,i} = \sigma_{e,i-1} + H_i\,\Delta\varepsilon^P_e \tag{24}$$

Defining $d\lambda$ (>0) as

$$d\lambda = 1 - \frac{\sigma_{e,i}}{3G\varepsilon_{et}} \tag{25}$$

the individual plastic strain increments are calculated as

$$\Delta\boldsymbol{\varepsilon}^P = d\lambda\boldsymbol{e} \tag{26}$$

or, to make the treatment general so that it can be applied to viscoplastic problems as well, the preceding equation can be replaced with

$$\dot{\boldsymbol{\varepsilon}}^P = \frac{d\lambda\boldsymbol{e}}{\Delta t} \tag{27}$$

VI. Algorithm

For the sake of completeness, the details of the algorithm used to produce the numerical results of the present study are presented here. To make the description general enough so that it also can be used in the context of viscoplasticity, all variables are assumed to be functions of time. It is therefore assumed that a history of effective strain rates $\dot{\bar{\varepsilon}}_i$ is available. The strain rates play the role of a driving force or load for the algorithm.

A. Core

1) Assemble Eqs. (1), i.e., $\boldsymbol{A}_G\boldsymbol{\varepsilon}_s = \boldsymbol{J}\bar{\boldsymbol{\varepsilon}}$ from displacement compatibility.

2) Assemble Eqs. (2), i.e., $\boldsymbol{A}_M\boldsymbol{\varepsilon}_s = \boldsymbol{0}$ from traction continuity.

3) Assemble matrices $\boldsymbol{A}$ and $\boldsymbol{K}$ [Eqs. (4) and (5)].

4) Find $\boldsymbol{A}_s = \boldsymbol{A}^{-1}\boldsymbol{K}$.

5) Compute the initial effective stiffness matrix:

$$\bar{\boldsymbol{C}}_0 \equiv \frac{1}{hl}\sum_{\beta}^{N_\beta}\sum_{\gamma}^{N_\gamma} h_\beta l_\gamma \boldsymbol{C}^{(\beta\gamma)}\boldsymbol{A}_s^{(\beta\gamma)}$$

6) Initialize variables and start loading cycle, i.e., set $i = 0$; $\sigma_{e,i} = \sigma_y$; $\bar{\boldsymbol{C}}^P = \bar{\boldsymbol{C}}_0$; $\bar{\boldsymbol{\sigma}}_i = \boldsymbol{0}$; $\bar{\boldsymbol{\varepsilon}}_i = \boldsymbol{0}$; $\bar{\boldsymbol{\varepsilon}}^P_i = \boldsymbol{0}$. Also, for all subcells do $\boldsymbol{\sigma}_i = \boldsymbol{0}$; $\boldsymbol{\varepsilon}_i = \boldsymbol{0}$; $\boldsymbol{\varepsilon}^P_i = \boldsymbol{0}$; $\Delta\boldsymbol{\varepsilon}^P_i = \boldsymbol{0}$.

a) Increment i: $i = i + 1$.

b) Find the new plastic strain in the composite: $\bar{\boldsymbol{\varepsilon}}^P_i = \bar{\boldsymbol{\varepsilon}}_{i-1} - \bar{\boldsymbol{C}}_0^{-1}\bar{\boldsymbol{\sigma}}_{i-1}$ [Eq. (18)].

c) Increment load: $\bar{\boldsymbol{\varepsilon}}_i = \bar{\boldsymbol{\varepsilon}}_{i-1} + \dot{\bar{\boldsymbol{\varepsilon}}}_i\Delta t$.

d) Find new effective stress: $\dot{\bar{\boldsymbol{\sigma}}}_i = \bar{\boldsymbol{C}}^P\dot{\bar{\boldsymbol{\varepsilon}}}_i$; $\bar{\boldsymbol{\sigma}}_i = \bar{\boldsymbol{\sigma}}_{i-1} + \dot{\bar{\boldsymbol{\sigma}}}_i\Delta t$.

e) Initialize plasticity iteration counter, i.e., set $j = 0$ and perform plasticity iterations according to Sec. VI.A.

f) For all subcells do

$$\sigma_{e,i-1} = \sigma_{e,i}, \qquad \boldsymbol{\sigma}_{i-1} = \boldsymbol{\sigma}_i, \qquad \boldsymbol{\varepsilon}_{i-1} = \boldsymbol{\varepsilon}_i$$

$$\boldsymbol{\varepsilon}^P_{i-1} = \boldsymbol{\varepsilon}^P_i, \qquad \boldsymbol{\varepsilon}^P_{e,i-1} = \boldsymbol{\varepsilon}^P_{e,i}$$

g) If $i <$ maximum number of load steps, go to a).

7) STOP

B. Plasticity Iterations

1) Increment j: $j = j + 1$.

a) For all subcells do

i) Calculate strain rates in the subcell using the current concentration matrix $\boldsymbol{A}_s$, i.e., $\dot{\boldsymbol{\varepsilon}}_i = \boldsymbol{A}_s\dot{\bar{\boldsymbol{\varepsilon}}}_i$.

ii) Find new strains and new stresses in the subcell, i.e., $\boldsymbol{\varepsilon}_i = \boldsymbol{\varepsilon}_{i-1} + \dot{\boldsymbol{\varepsilon}}_i\Delta t$; $\bar{\boldsymbol{\sigma}}_i = \bar{\boldsymbol{C}}_0(\bar{\boldsymbol{\varepsilon}}_i - \bar{\boldsymbol{\varepsilon}}^P_{i-1})$.

iii) Obtain $\varepsilon^P_{e,i}$, $\Delta\varepsilon^P_{e,i}$, and $\dot{\boldsymbol{\varepsilon}}^P_i$ following the procedure outlined in Sec. V.

iv) Update the plastic strain $\boldsymbol{\varepsilon}^P_i = \boldsymbol{\varepsilon}^P_{i-1} + \dot{\boldsymbol{\varepsilon}}^P_i\Delta t$.

v) Calculate the subcell deviatoric stresses $\boldsymbol{s}$ [Eq. (17)].

vi) Update the subcell tangent plasticity matrix as[5]

$$\boldsymbol{C}^{P(\beta\gamma)} = \boldsymbol{C}_0^{(\beta\gamma)} - \frac{\left[\boldsymbol{C}_0^{(\beta\gamma)}\dot{\boldsymbol{\varepsilon}}^P\right]\boldsymbol{s}^T}{\dot{\boldsymbol{\varepsilon}}^T\boldsymbol{s}}$$

b) Reassemble $\boldsymbol{A}$ using the new subcell plasticity matrices $\boldsymbol{C}^P$.

c) Find the current $\boldsymbol{A}_s$: $\boldsymbol{A}_s = \boldsymbol{A}^{-1}\boldsymbol{K}$.

d) Compute current effective plastic stiffness matrix [Eq. (15)]:

$$\bar{\boldsymbol{C}}^P \equiv \frac{1}{hl}\sum_{\beta}^{N_\beta}\sum_{\gamma}^{N_\gamma} h_\beta l_\gamma \boldsymbol{C}^{P(\beta\gamma)}\boldsymbol{A}_s^{(\beta\gamma)}$$

e) Check for convergence of the plasticity iteration procedure. For some convenient tolerance parameters δ_1 and δ_2 do for all subcells

i) $\delta_1 = \Delta\varepsilon^P_{e,i} - \Delta\varepsilon^P_{e,i-1}$.

ii) Set $\Delta\varepsilon^P_{e,i-1} = \Delta\varepsilon^P_{e,i}$ for all subcells.

iii) If for any subcell $\delta_1 > \delta_2\varepsilon^P_{e,i}$, go to 1.

2) End.

VII. Computational Aspects

As mentioned in Sec. IV, to solve a single plasticity problem it is necessary to solve the linear system(s) represented by Eq. (6) hundreds of times. A single (sparse) factorization of $\boldsymbol{A}$ plus the corresponding backward and forward passes to find $\boldsymbol{A}_s$ takes approximately 39 s of CPU time on an SGI Indigo2 workstation. For a problem with 10,000 subcells, the matrix $\boldsymbol{A}$ has 238,938 nonzero entries. In a typical plasticity problem with 10,000 subcells, Eq. (6) is solved approximately 850 times. This takes about 9 h of CPU time on an SGI Indigo2 workstation. Some typical results and comparisons between the tangent-sparse implementation and the original implementation of the GMC are shown in Table 1.

Table 1 Performance comparison between the original (dense) implementation of the GMC and the new tangent-sparse implementation for a typical plasticity problem

Subcell arrangement	No. of subcells	CPU, s		Speed up
		Original (dense)	Tangent sparse	
4×4	16	149	2.14	69.6
10×10	100	76,278	27	2,825
50×50	2,500	—	3,317	—
100×100	10,000	—	30,830	—

VIII. Numerical Results

To show the computational power of the new tangent-sparse GMC formulation, several numerical experiments were performed with microstructures modeled using a large number of subcells. The cell microstructures chosen for the sample problems differed in either fiber shape or fiber architecture. The results not only demonstrate the computational power of the new GMC formulation but also confirm the results of previous studies about the influence of fiber shape and fiber architecture on the nonlinear behavior of unidirectional composites.[7–10] In addition, the results of the present study shed more light on the subject because the new formulation makes it possible to model any given microstructure with a larger degree of detail.

Boron/aluminum composite microstructures were used in all numerical experiments. The engineering properties of the materials used (aluminum and boron) were obtained from Ref. 2 and are presented in Table 2.

The effect of scale and/or refinement of the microstructure on the elastic response of unidirectional composites was demonstrated in Ref. 4. The effect of scale and refinement of the microstructure on the plastic response of unidirectional composites is illustrated here by means of the first numerical experiment. Four different unit cells with random microstructures with 10×10, 15×15, 50×50, and 100×100 subcells, respectively, were used. These unit cells are shown in Fig. 3. The boron volume fraction used was 0.7. In Fig. 3 and all other figures the boron material is shown in dark. The response of the aluminum phase was taken as bilinear with a strain-hardening slope equal to 5% of the aluminum Young modulus. Because of the high volume fraction of the boron material, the microstructures shown in Fig. 3 can be regarded as RVE of a unidirectional composite having a ceramic matrix (boron) with ductile inclusions (aluminum) rather than the other way around. The plastic responses (transverse normal stresses σ_{22} and σ_{33}) of the microstructures shown in Fig. 3 are presented in Fig. 4. Because the randomness of a unit cell increases as the number of subcells increases, the responses for σ_{22} and σ_{33} tend to coincide as the number of subcells increases. In fact, all curves in Fig. 4 practically coincide for arrays of 50×50 subcells or more. The fact that the responses for σ_{33} and σ_{22} coincide for large numbers of subcells suggests that these microstructures exhibit transversely isotropic behavior as the number of random inclusions increases.

Table 2 Material properties of boron/aluminum composite used in the numerical experiments (from Ref. 1.)

Material	Young's modulus, GPa	Poisson's ratio
Boron	413.16	0.2
Aluminum	55.16	0.3

The second numerical experiment involves again a boron/aluminum composite with elliptical and circular fibers. The unit cells corresponding to this case are shown in Fig. 5 together with the corresponding plastic responses. There is a clear difference in the responses because of the difference in shape. This difference is observed only for the case when there is some strain hardening in the aluminum. The results shown in Fig. 5 correspond to a fiber volume fraction of 0.28 and a strain-hardening slope equal to 5% of the modulus of elasticity of the aluminum. For zero strain hardening the two responses practically coincide (for this particular volume fraction).

The third numerical experiment involved a set of five different microstructures with a fiber volume fraction of 0.4 (Figs. 6 and 7; the square-edge packing shown in Fig. 6 is equivalent to the single circular fiber shown in Fig. 7). Transverse responses for these microstructures were determined using zero and 15% hardening. The responses corresponding to zero hardening are shown in Fig. 8.

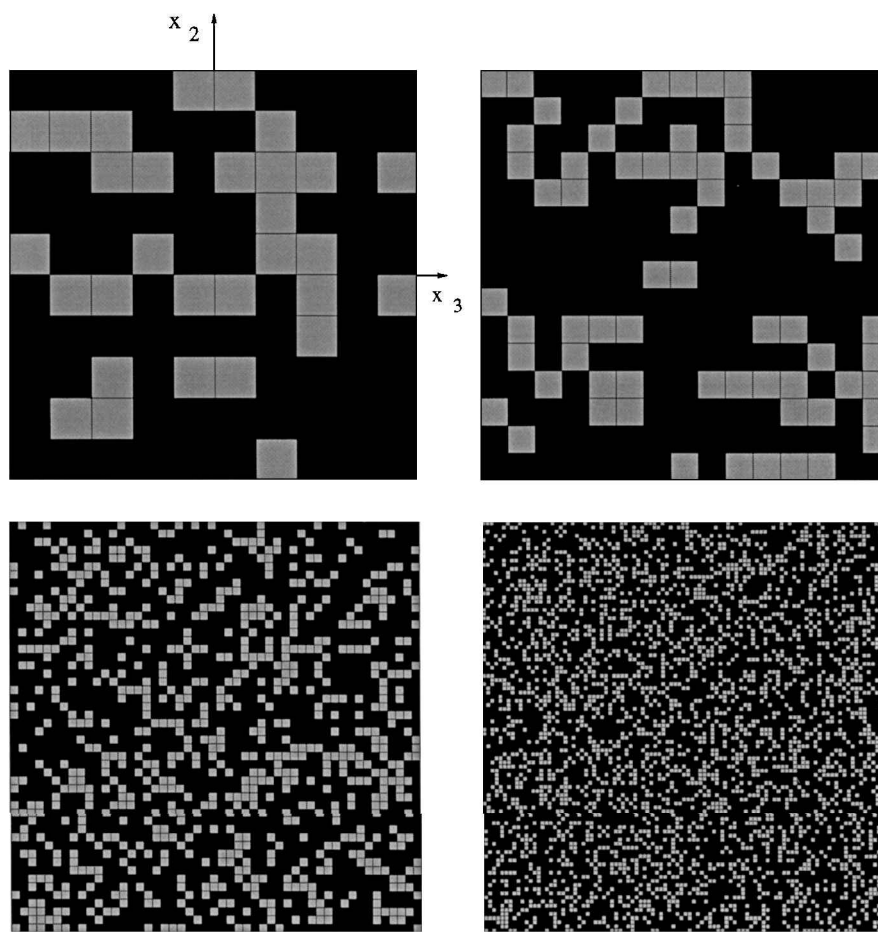

Fig. 3 Boron/Al composite microstructures with random inclusions. Boron shown in dark. Boron volume fraction: 0.7 (aluminum volume fraction: 0.3). Cell arrays shown are 10×10, 15×15, 50×50, and 100×100.

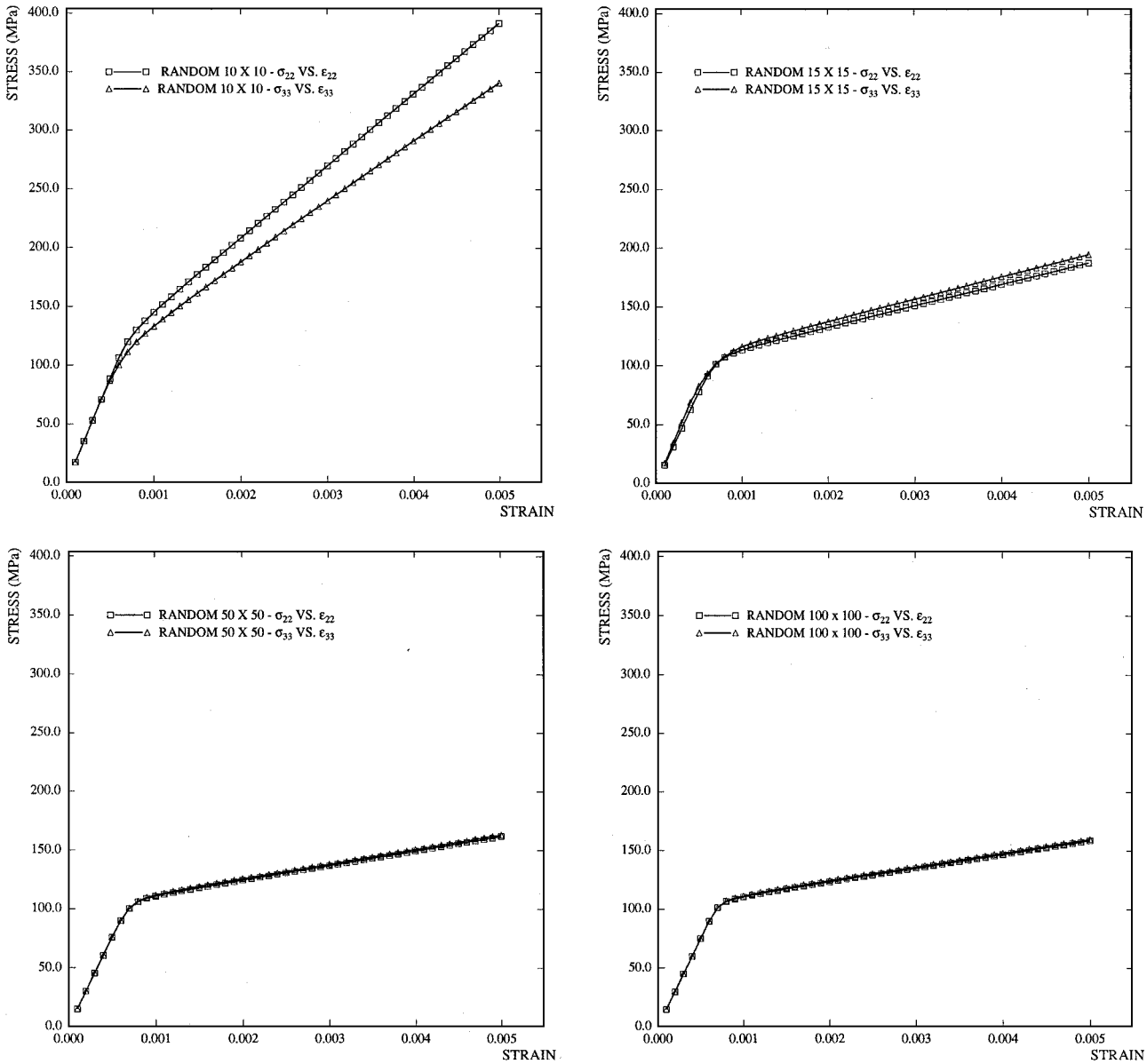

Fig. 4 Plastic responses of the boron/Al microstructures shown in Fig. 3. Boron volume fraction: 0.7. Strain hardening for the aluminum phase: 5% of Young's modulus.

The hexagonal, the square-diagonal, and the random microstructures produce essentially the same response. The circular fiber produces a slightly different response, the most significant feature of which is the fact that its transverse elastic modulus (E_{22}) is about 10% higher than that of the random microstructure. The square fiber presents a response with a long hardening region and a much higher composite yield stress. This response agrees well with that reported in Ref. 9, where a simple 2×2 subcell array and the initial stiffness matrix approach were used.

The responses corresponding to 15% hardening are shown in Fig. 9. The responses corresponding to the square-diagonal, hexagonal, and random patterns differ little and present the lowest composite hardening slope; this is an expected result because hexagonal and square-diagonal packing closely emulate transversely isotropic behavior such as that exhibited by a composite with a large number of random inclusions.[4] The highest hardening slope is observed for the square-edge packing. (This packing is equivalent to one single fiber in the center of the unit cell, such as the one shown in Fig. 7.) Despite differences in the methodology and minor differences in the material properties, the responses for the square-edge, hexagonal, and square-diagonal packing qualitatively agree with those reported in Ref. 8. The result corresponding to the random packing does not agree well and could be explained by the smaller number of random inclusions used in Ref. 8. However, as already mentioned, the response obtained here for the random packing practically coincides with those of the hexagonal and square-diagonal arrays, as might be expected.

As mentioned in the Introduction, the GMC has been proven to produce accurate results for the effective properties and macroscopic behavior of a variety of composites under a variety of mechanical and thermal loading conditions.[3] The GMC also has been used successfully in predicting the influence of fiber architecture and fiber shape, as was done in Ref. 10 and the present study. Because of the averaging nature of the equations, however, the GMC is incapable of capturing the stress concentrations that will be present at, for example, the corners of a microstructure with a square fiber. To obtain accurate results in these cases, more sophisticated methods such as the finite element method (FEM) must be used. A comparison of results obtained with the GMC and the FEM when applied to the problem of determining residual stresses in a metal matrix composite can be found in Ref. 11. In Ref. 11 the stresses in the metal matrix predicted by the GMC were less accurate than those predicted by the FEM. However, in Ref. 11 the average matrix stresses predicted by the two methods were comparable. A comparison of the relative computational costs of the GMC and the FEM when applied to the problem of determining the viscoplastic response of

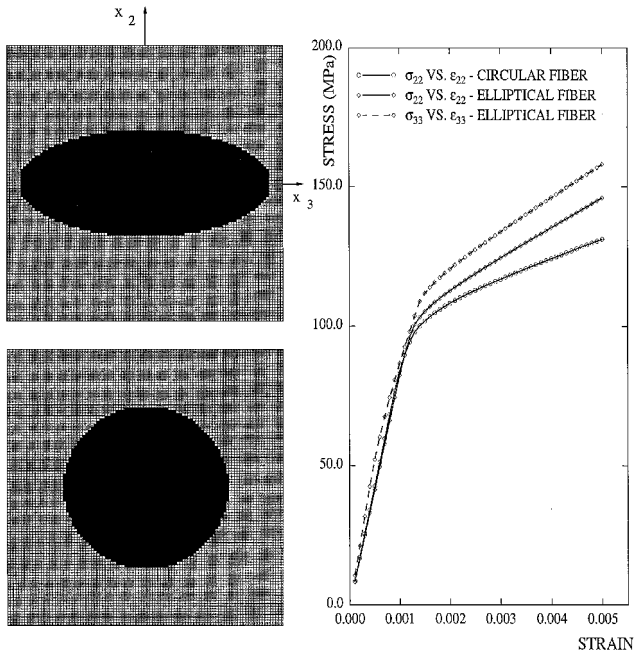

Fig. 5 Boron/Al composite microstructures that differ only in fiber shape. Fiber material: boron. Fiber volume fraction: 0.28. Aspect ratio of elliptical fiber: 2.3. Cell model with 10,000 subcells. Strain hardening for the aluminum phase: 5% of Young's modulus.

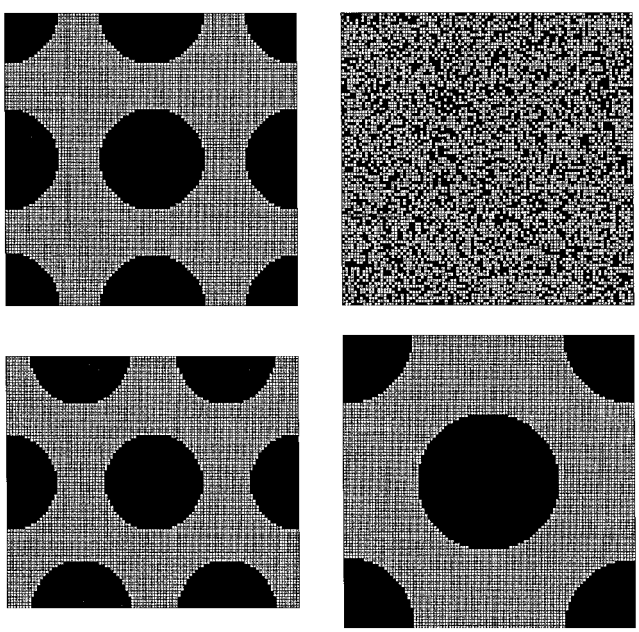

Fig. 6 Upper-left-hand corner, square-edge packing of circular fibers; upper-right-hand corner, randomly distributed fiber material; lower-left-hand corner, hexagonal (triangular) packing of circular fibers; and lower-right-hand corner, square-diagonal packing of circular fibers. Fiber material: boron. Fiber volume fraction: 0.4.

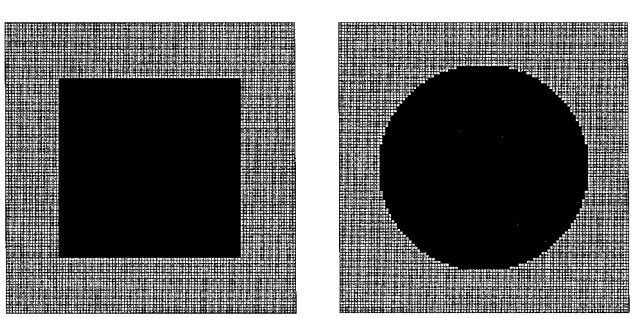

Fig. 7 Boron/Al microstructures with square and circular fibers. Fiber material: boron. Fiber volume fraction: 0.4.

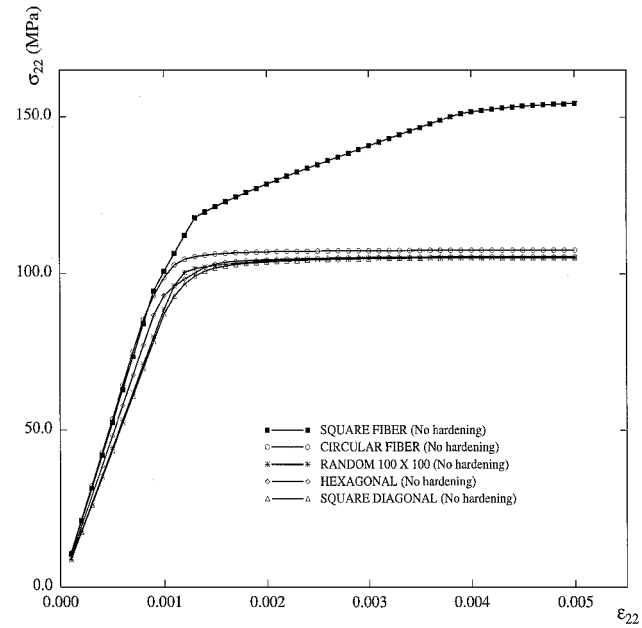

Fig. 8 Plastic responses of the boron/Al composite microstructures shown in Figs. 6 and 7. Fiber volume fraction: 0.4. Perfect elastic-plastic model for the aluminum phase (no strain hardening).

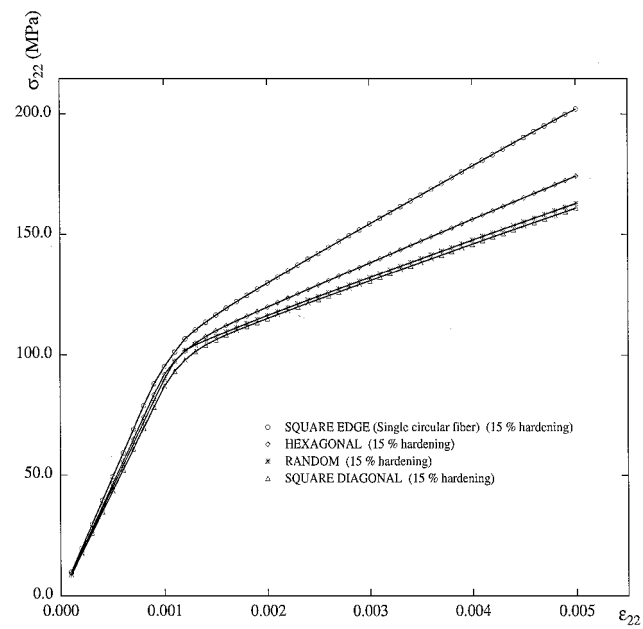

Fig. 9 Responses of the boron/Al composite microstructures of Figs. 6 and 7 for the case with hardening. Hardening for the aluminum phase: 15% of Young's modulus.

a composite can be found in Ref. 12. To obtain with the FEM the same accuracy of a 49-subcell GMC model, 1088 finite elements are needed.[12] This makes the FEM considerably more costly than the GMC. Using the FEM for micromechanical analysis has other shortcomings. For instance, it is necessary to appropriately model the boundary conditions of a boundary-value problem to obtain effective properties and/or stresses. In addition, it is usually necessary to use three-dimensional finite elements to model all possible loading conditions.

IX. Concluding Remarks

A new formulation of the GMC that can be used to advantage in modeling the linear and nonlinear, e.g., plastic, behavior of unidirectional composites with complex microstructures has been presented. The formulation makes use of the so-called tangent plasticity matrix approach and takes advantage of the sparsity of the GMC's main matrices. It is especially suited to problems that require high-resolution

unit cell models. In particular, plastic micromechanical analyses of composites with up to 10,000 subcells have been performed. The effects of scale (or refinement) of the microstructure on the plastic response of unidirectional composites were studied by using random microstructures with an increasing number of subcells. As the number of subcells is increased, the behavior of these random microstructure composites tends to that of a transversely isotropic material, as might be expected. Some other results from previous studies about the influence of fiber shape and fiber architecture on the plastic response of composites were confirmed. In addition, it was found that, in the absence of strain hardening, the differences in plastic response for many fiber distribution patterns are small, and differences start to become important only when the matrix phase exhibits some strain hardening. On the other hand, microstructures with square fibers present significantly different plastic responses even in the absence of strain hardening.

References

[1]Paley, M., and Aboudi, J., "Micromechanical Analysis of Composites by the Generalized Method of Cells," *Mechanics of Materials*, Vol. 14, No. 2, 1992, pp. 127–139.

[2]Aboudi, J., *Mechanics of Composite Materials—A Unified Micromechanical Approach*, Elsevier, Amsterdam, 1991, pp. 35–53.

[3]Aboudi, J., "Micromechanical Analysis of Composites by the Method of Cells—Update," *Applied Mechanics Reviews*, Vol. 49, No. 10, 1996, pp. 583–591.

[4]Orozco, C. E., "Computational Aspects of Modeling Complex Microstructure Composites Using GMC," *Composites Engineering*, Vol. 28B, No. 1/2, 1997, pp. 167–175.

[5]Paley, M., and Aboudi, J., "Viscoplastic Bifurcation Buckling of Plates," *AIAA Journal*, Vol. 29, No. 4, 1991, pp. 627–632.

[6]Mendelson, A., *Plasticity: Theory and Application*, Krieger, Malabar, FL, 1983, pp. 123–127.

[7]Brockenbrough, J. R., and Suresh, S., "Plastic Deformation of Continuous Fiber-Reinforced Metal-Matrix Composites: Effects of Fiber Shape and Distribution," *Scripta Metallurgica et Materialia*, Vol. 24, No. 2, 1990, pp. 325–330.

[8]Brockenbrough, J. R., Suresh, S., and Wienecke, H. A., "Deformation of Metal-Matrix Composites with Continuous Fibers: Geometrical Effects of Fiber Distribution and Shape," *Scripta Metallurgica et Materialia*, Vol. 39, No. 5, 1991, pp. 735–752.

[9]Sankurathri, A., Baxter, S., and Pindera, M.-J., "The Effect of Fiber Architecture on the Inelastic Response of Metal Matrix Composites with Interfacial and Fiber Damage," *Damage and Interfacial Debonding in Composites*, edited by G. Z. Voyiadjis and D. H. Allen, Elsevier Science, Amsterdam, 1996, pp. 235–257.

[10]Arnold, S. M., Pindera, M.-J., and Wilt, T. E., "Influence of Fiber Architecture on the Elastic and Inelastic Response of Metal Matrix Composites," *International Journal of Plasticity*, Vol. 12, No. 4, 1996, pp. 507–545.

[11]Brayshaw, J. M., and Pindera, M.-J., "The Effect of the Matrix Constitutive Model on Residual Thermal Stresses in MMC," *Mechanics of Composites at Elevated and Cryogenic Temperatures*, edited by S. N. Singhal, W. F. Jones, and C. T. Herakovich, Vol. 118, American Society of Mechanical Engineers, Applied Mechanics Div., New York, 1991, pp. 23–38.

[12]Wilt, T. E., "On the Finite Element Implementation of the Generalized Method of Cells Micromechanics Constitutive Model," NASA CR-195451, March 1995.

A. M. Waas
Associate Editor